

## Charged-current deep-inelastic scattering of muon neutrinos ( $\nu_\mu$ ) off $^{56}\text{Fe}$

Deepika Grover,<sup>1,\*</sup> Kapil Saraswat,<sup>1,†</sup> Prashant Shukla,<sup>2,3,‡</sup> and Venktesh Singh<sup>1,§</sup>

<sup>1</sup>*Department of Physics, Institute of Science, Banaras Hindu University, Varanasi 221005, India*

<sup>2</sup>*Nuclear Physics Division, Bhabha Atomic Research Centre, Mumbai 400085, India*

<sup>3</sup>*Homi Bhabha National Institute, Anushakti Nagar, Mumbai 400094, India*



(Received 1 August 2018; published 13 December 2018)

In this paper, we study charged-current deep-inelastic scattering of muon neutrinos off  $^{56}\text{Fe}$  nuclei by using the Hirai, Kumano, and Saito model. The LHA parton distribution functions (PDFs) - CT10 are used to describe the partonic content of hadrons. Modification of PDFs inside the nuclei is done by using EPPS16 parametrization at next-to-leading order. Target mass correction has also been incorporated in the calculations. We calculate the structure functions [ $F_2(x, Q^2)$  and  $x F_3(x, Q^2)$ ], the ratios [ $R_2(x, Q^2) = F_2^{^{56}\text{Fe}}/F_2^{\text{Nucleon}}$  and  $R_3(x, Q^2) = F_3^{^{56}\text{Fe}}/F_3^{\text{Nucleon}}$ ], and the differential cross sections of  $\nu_\mu$  deep-inelastic scattering off nucleons and  $^{56}\text{Fe}$  nuclei. We compare the results obtained with measured experimental data. The present theoretical approach gives a good description of data.

DOI: [10.1103/PhysRevC.98.065503](https://doi.org/10.1103/PhysRevC.98.065503)

### I. INTRODUCTION

In the standard model of physics, neutrinos are elementary particles with no electric charge, no magnetic moment, half-integral spin, and zero mass. However, several neutrino oscillation experiments [1–10] across the globe have confirmed that neutrinos oscillate from one flavor to another, leading to a small but nonzero neutrino mass and the possibility to go beyond the standard model. Being electrically neutral, neutrinos rarely interact with matter via the weak force. Neutrino interactions are classified into two categories: Charged current (CC) interactions via the exchange of  $W^+/W^-$  bosons and neutral current (NC) interactions via the exchange of  $Z$  bosons. There are many neutrino-scattering processes such as quasi-elastic-scattering (QES) [11], resonance pion production (RES) [12], and deep-inelastic scattering (DIS), at various neutrino energies; for a review see Refs. [13,14]. Low neutrino energies are dominated by QES whereas RES dominates at medium neutrino energies. As the neutrino energies become larger, DIS becomes more and more dominant [15]. In this scattering process, a highly energetic neutrino scatters off a quark in the nucleon producing a corresponding lepton, and

many hadrons are produced:

$$\nu_\mu + N \rightarrow \mu^- + X \text{ (CC)}, \quad (1)$$

$$\nu_\mu + N \rightarrow \nu_\mu + X \text{ (NC)}. \quad (2)$$

DIS is an important experimental tool for studying the hadronic matter where the final-state particles produced in the scattering are analyzed to probe hadronic properties. Several experiments planned worldwide, such as NuTeV [16], CHORUS [17], NOMAD [18], MINOS [19], MINERvA [20], etc., have analyzed neutrino deep-inelastic scattering off different targets to measure differential and integrated cross sections and structure functions. A review of the results from various experiments probing neutrino deep-inelastic scattering is presented in Ref. [21].

To describe the partonic content of the hadron, precise parton distribution functions (PDFs) are required. These PDFs are produced by several different groups, such as MRST [22–24], CTEQ [25], Alekhin [26,27], ZEUS [28], etc. PDFs are derived from fitting DIS and related hard-scattering data by using parametrization at low  $Q_0^2$  [1–7  $(\text{GeV}/c)^2$ ] and evolving these to higher  $Q^2$ . These PDFs are presented as grids in  $x$ - $Q^2$  with codes given by PDF authors. The Les Houches Accord PDFs (LHAPDF) provides C++ code for these PDFs with an interpolation grid build into the PDFLIB [29]. We use LHAPDF (CT10) [30] parton distribution functions.

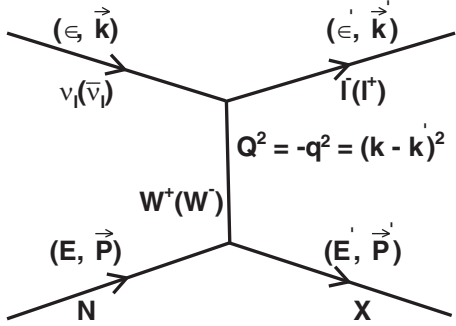
In this work, we study charged current  $\nu_\mu$ —nucleon and  $\nu_\mu$ — $^{56}\text{Fe}$  deep-inelastic scattering by using the Hirai, Kumano, and Saito model [31]. Calculations of the structure functions [ $F_2(x, Q^2)$  and  $x F_3(x, Q^2)$ ], the ratios [ $R_2(x, Q^2) = F_2^{^{56}\text{Fe}}/F_2^{\text{Nucleon}}$  and  $R_3(x, Q^2) = F_3^{^{56}\text{Fe}}/F_3^{\text{Nucleon}}$ ], and the differential cross sections are presented and compared with the measured experimental data.

\*dgroverbhu@gmail.com

†kapilsaraswatbhu@gmail.com

‡pshuklabarc@gmail.com

§venkaz@yahoo.com

FIG. 1. Charged current  $\nu$ - $N$  deep-inelastic scattering.

## II. FORMALISM FOR DEEP-INELASTIC $\nu$ - $N$ AND $\nu$ - $A$ SCATTERING

The neutrino-nucleon (antineutrino-nucleon) deep-inelastic scattering process is

$$\nu_l(k) + N(P) \rightarrow l^-(k') + X(P'), \quad (3)$$

$$\bar{\nu}_l(k) + N(P) \rightarrow l^+(k') + X(P'), \quad (4)$$

where neutrino or antineutrino with four-momentum  $k = (\epsilon, \vec{k})$  scatters off a nucleon  $N$  with four-momentum  $P^\mu = (E, \vec{P})$  and  $E = (M^2 + \vec{P}^2)^{1/2}$ . The outgoing lepton  $l^-$  or  $l^+$  (not neutrino) has four-momentum  $k' = (\epsilon', \vec{k}')$ . The hadronic final state  $X$  is left with a four-momentum  $P' = (E', \vec{P}')$ . The schematic diagram of charged current  $\nu$ - $N$  deep-inelastic scattering is shown in Fig. 1.

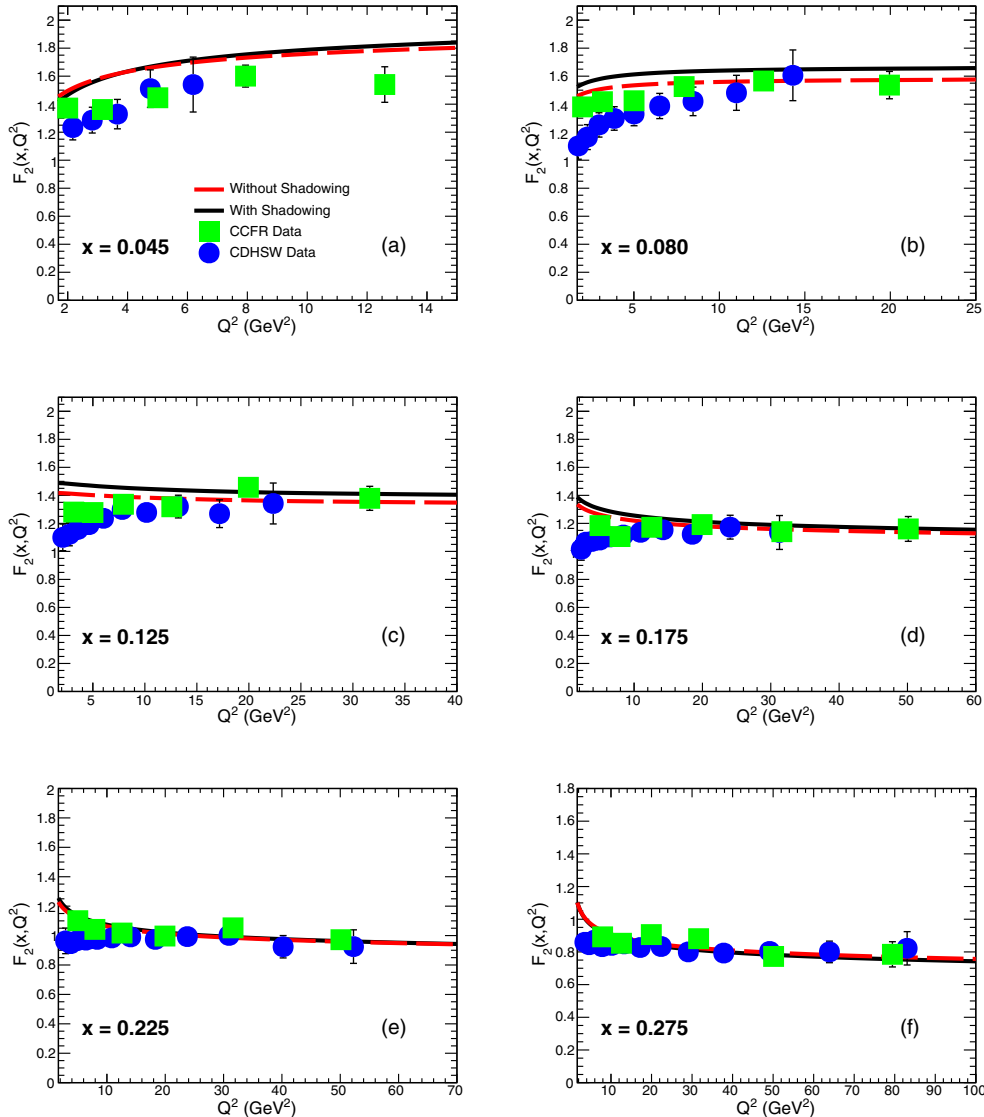


FIG. 2.  $F_2(x, Q^2)$  with EPPS16 nuclear corrections [37] at NLO and LHAPDF (CT10) parton distribution functions [30] for  $^{56}\text{Fe}$  as a function of  $Q^2$  for different values of Bjorken variable  $x$ . The results are compared with measured data of CDHSW [39] and CCFR [40] experiments.

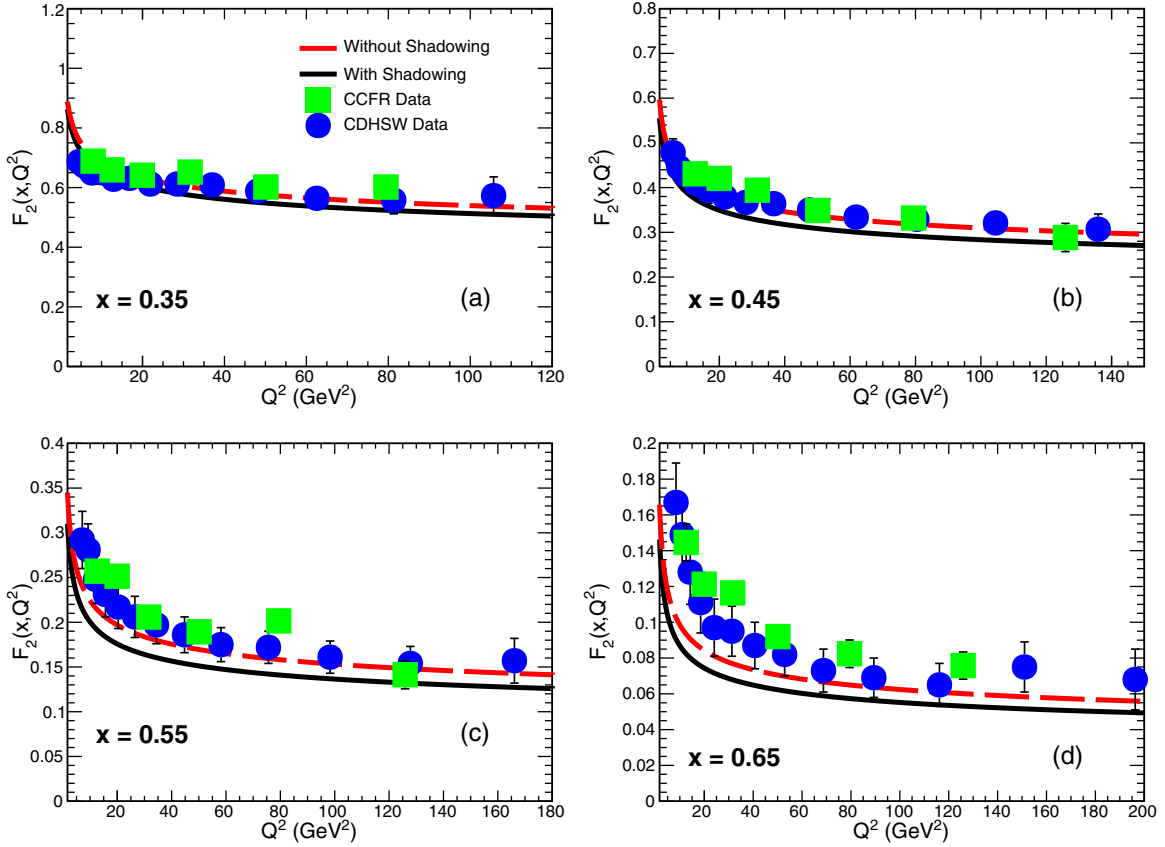


FIG. 3.  $F_2(x, Q^2)$  with EPPS16 nuclear corrections [37] at NLO and LHAPDF (CT10) parton distribution functions [30] for  $^{56}\text{Fe}$  as a function of  $Q^2$  for different values of Bjorken variable  $x$ . The results are compared with measured data of CDHSW [39] and CCFR [40] experiments.

Neutrino CC (charged current) interactions with nucleon are described by the matrix elements [31]

$$M = \frac{G_F}{\sqrt{2}} \frac{M_W^2}{M_W^2 + Q^2} \bar{u}(k', \lambda') \times \gamma^\mu (1 - \gamma_5) u(k, \lambda) \langle X | J_\mu^{CC}(0) | P, \lambda_N \rangle, \quad (5)$$

where  $G_F$  is the Fermi coupling constant,  $M_W$  is the  $W$  mass,  $Q^2$  is given by  $Q^2 = -q^2 = (k - k')^2$  with the four-momentum transfer  $q$ ,  $k(\lambda)$ , and  $k'(\lambda')$  indicate initial and final lepton momenta (spins),  $P(\lambda_N)$  is the nucleon momentum (spin), and  $J_\mu^{CC}(0)$  is the weak charged current (CC) of the nucleon. The absolute value square  $|M|^2$  is calculated with an average over the nucleon spin for obtaining the differential cross section.

The neutrino-nucleon (antineutrino-nucleon) charged current differential scattering cross section is defined as [31]

$$\begin{aligned} \frac{d^2\sigma_{CC}^{\nu(\bar{\nu})}}{dxdy} = & \frac{G_F^2 M_N E_\nu}{\pi} \left( \frac{M_W^2}{M_W^2 + Q^2} \right)^2 \left[ F_1(x, Q^2) xy^2 \right. \\ & + F_2(x, Q^2) \left( 1 - y - \frac{M_N xy}{2E_\nu} \right) \\ & \left. \pm F_3(x, Q^2) xy \left( 1 - \frac{y}{2} \right) \right], \end{aligned} \quad (6)$$

where  $\pm$  indicates  $+$  for  $\nu$  and  $-$  for  $\bar{\nu}$ ,  $x$  is the Bjorken scaling variable defined as  $x = Q^2/(2P \cdot q)$ ,  $y$  is the inelasticity defined as  $y = P \cdot q/(P \cdot k)$ , so  $Q^2 = 2M_N E_\nu x y$ ,  $E_\nu$  is the neutrino-beam energy, and  $M_N$  is the nucleon mass.  $F_1(x, Q^2)$ ,  $F_2(x, Q^2)$ , and  $F_3(x, Q^2)$  are the dimensionless structure functions. The Bjorken variable  $x$  and the inelasticity  $y$  are in the range  $0 \leq x, y \leq 1$ .

In the Bjorken limit of scaling in the asymptotic region i.e.,  $Q^2 \rightarrow \infty$ ,  $x$  is finite. The structure functions  $F_i(x, Q^2)$  are not  $Q^2$  dependent but depend only on  $x$  and satisfy the Callan–Gross relation [32]:

$$F_2(x) = 2x F_1(x). \quad (7)$$

Using the Callan–Gross relation, the differential cross section can be expressed in terms of  $F_2$  and  $F_3$ . In the quark parton model (QPM),  $F_2(x, Q^2)$  and  $F_3(x, Q^2)$  are determined in terms of PDFs for quarks and antiquarks.

The structure function  $F_3(x, Q^2)$  is defined as

$$\begin{aligned} F_3^N(x, Q^2) = & (u(x, Q) - \bar{u}(x, Q) + d(x, Q) \\ & - \bar{d}(x, Q) + s(x, Q) - \bar{s}(x, Q) \\ & + c(x, Q) - \bar{c}(x, Q) + b(x, Q) \\ & - \bar{b}(x, Q) + t(x, Q) - \bar{t}(x, Q)). \end{aligned} \quad (8)$$

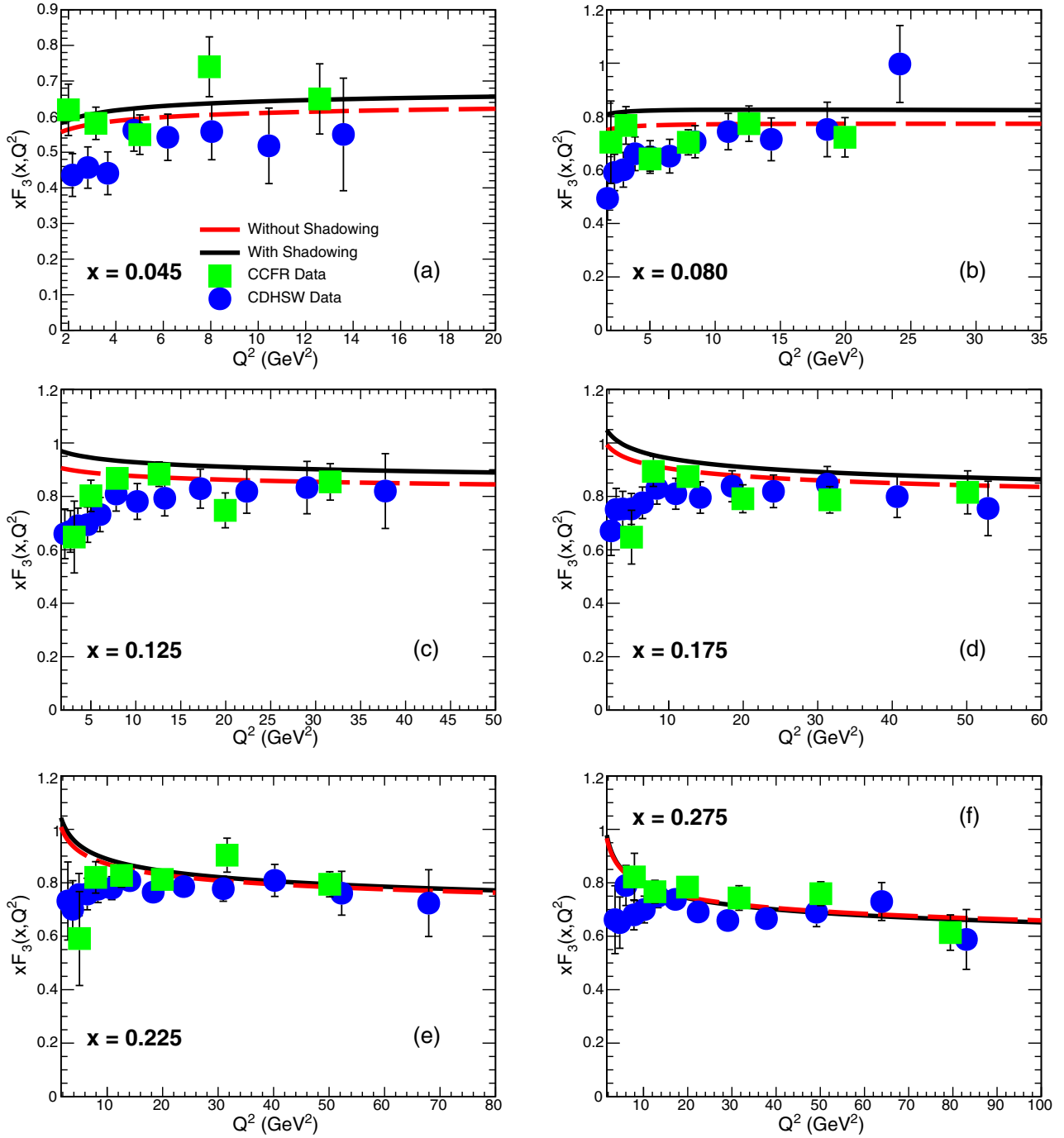


FIG. 4.  $x F_3(x, Q^2)$  with EPPS16 nuclear corrections [37] at NLO and LHAPDF (CT10) parton distribution functions [30] for  $^{56}\text{Fe}$  as a function of  $Q^2$  for different values of the Bjorken variable  $x$ . The results are compared with measured data of the CDHSW [39] and CCFR [40] experiments.

The structure function  $F_2(x, Q^2)$  is defined as

$$\begin{aligned} F_2^N(x, Q^2) = & x(u(x, Q) + \bar{u}(x, Q) + d(x, Q) \\ & + \bar{d}(x, Q) + s(x, Q) + \bar{s}(x, Q) \\ & + c(x, Q) + \bar{c}(x, Q) + b(x, Q) \\ & + \bar{b}(x, Q) + t(x, Q) + \bar{t}(x, Q)). \end{aligned} \quad (9)$$

### III. NUCLEAR MODIFICATIONS

There are some nuclear effects [33] in neutrino-nucleus deep-inelastic scattering processes. These effects were first pointed out in 1982 by the EMC collaboration at CERN, where they measured the ratio of the iron [ $F_2^A(x, Q^2)$ ] to deuterium [ $F_2^D(x, Q^2)$ ] structure functions, and found the results to be different from unity [34]. Several efforts since then have

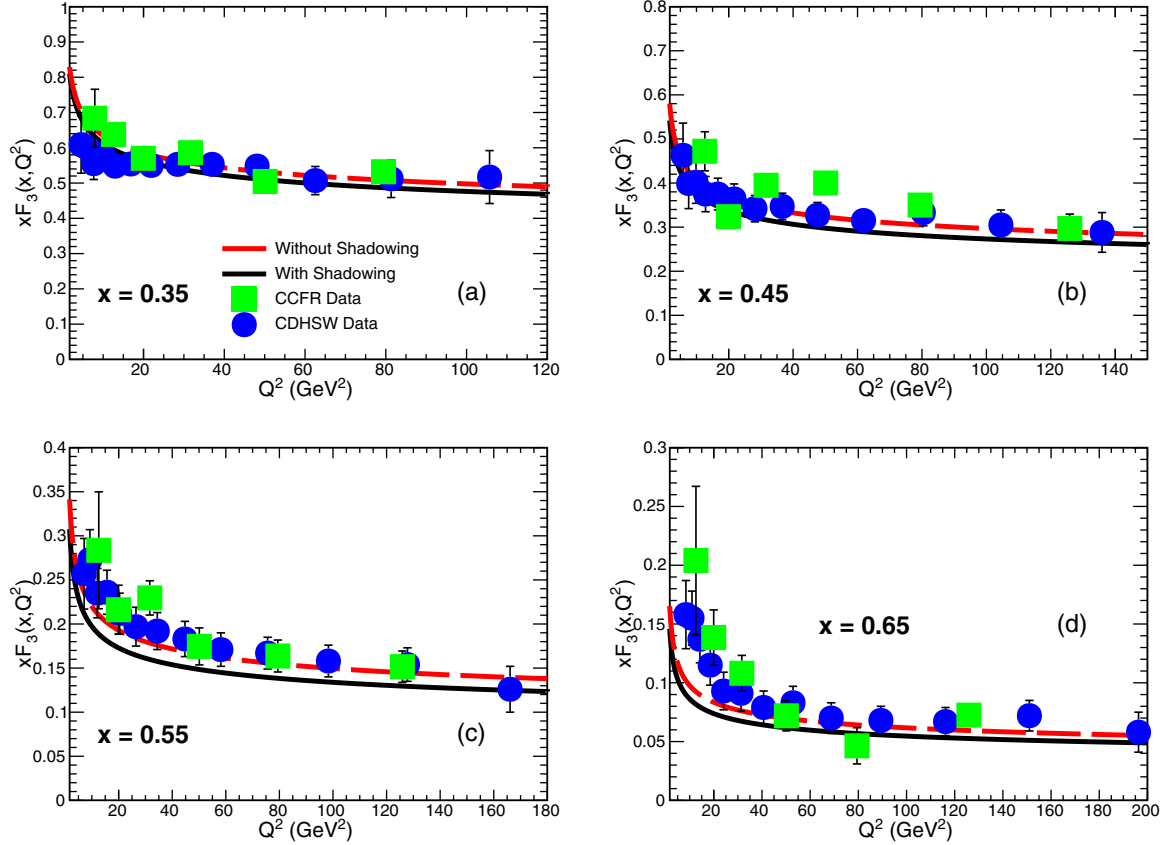


FIG. 5.  $x F_3(x, Q^2)$  with EPPS16 nuclear corrections [37] at NLO and LHAPDF (CT10) parton distribution functions [30] for  ${}^{56}\text{Fe}$  as a function of  $Q^2$  for different values of the Bjorken variable  $x$ . The results are compared with measured data of the CDHSW [39] and CCFR [40] experiments.

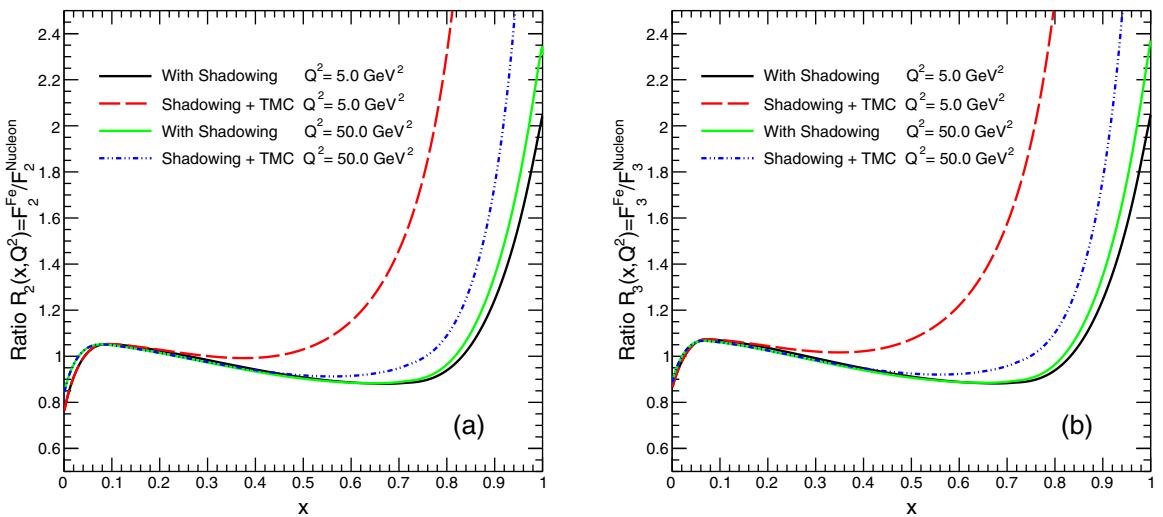


FIG. 6. Ratios (a)  $R_2(x, Q^2) = F_2^{{}^{56}\text{Fe}} / F_2^{\text{Nucleon}}$  and (b)  $R_3(x, Q^2) = F_3^{{}^{56}\text{Fe}} / F_3^{\text{Nucleon}}$  as a function of Bjorken variable  $x$  with EPPS16 nuclear corrections [37] at NLO and LHAPDF (CT10) parton distribution functions [30] for  $Q^2 = 5.0 \text{ GeV}^2$  and  $Q^2 = 50.0 \text{ GeV}^2$ .

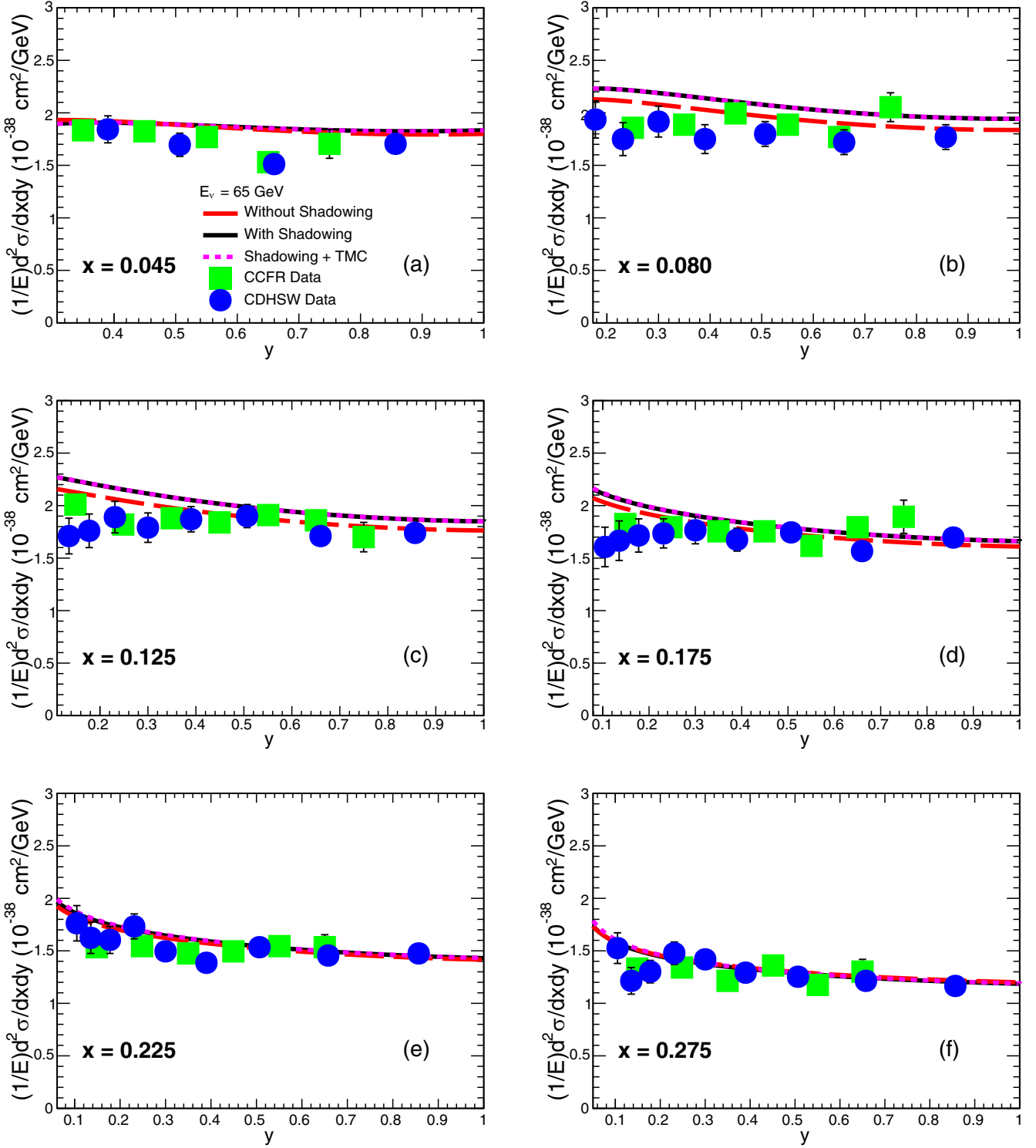


FIG. 7.  $\frac{1}{E} \frac{d^2\sigma}{dxdy}$  for  $^{56}\text{Fe}$  as a function of inelasticity  $y$ , for different values of the Bjorken variable  $x$  and  $E_{v_\mu} = 65$  GeV using EPPS16 nuclear corrections [37] at NLO and LHAPDF (CT10) parton distribution functions [30]. Results are compared with measured data of the CCFR [41] and CDHSW [41] experiments.

explored these effects in neutrino-nucleus DIS processes with the conclusion that, for a Bjorken variable  $x < 0.1$ , the ratio is suppressed and the suppression increases with increase in the mass number of the target nucleus. This suppression is called shadowing effect. For  $0.1 < x < 0.3$ , the ratio is more

than unity. This increase in the ratio is called antishadowing effect. For  $0.3 < x < 0.8$ , the ratio is again suppressed and this suppression is called EMC effect. For  $x > 0.8$ , the ratio increases rapidly and this rapid increase in the ratio is due to the Fermi motion effect. For a review, see Ref. [35].

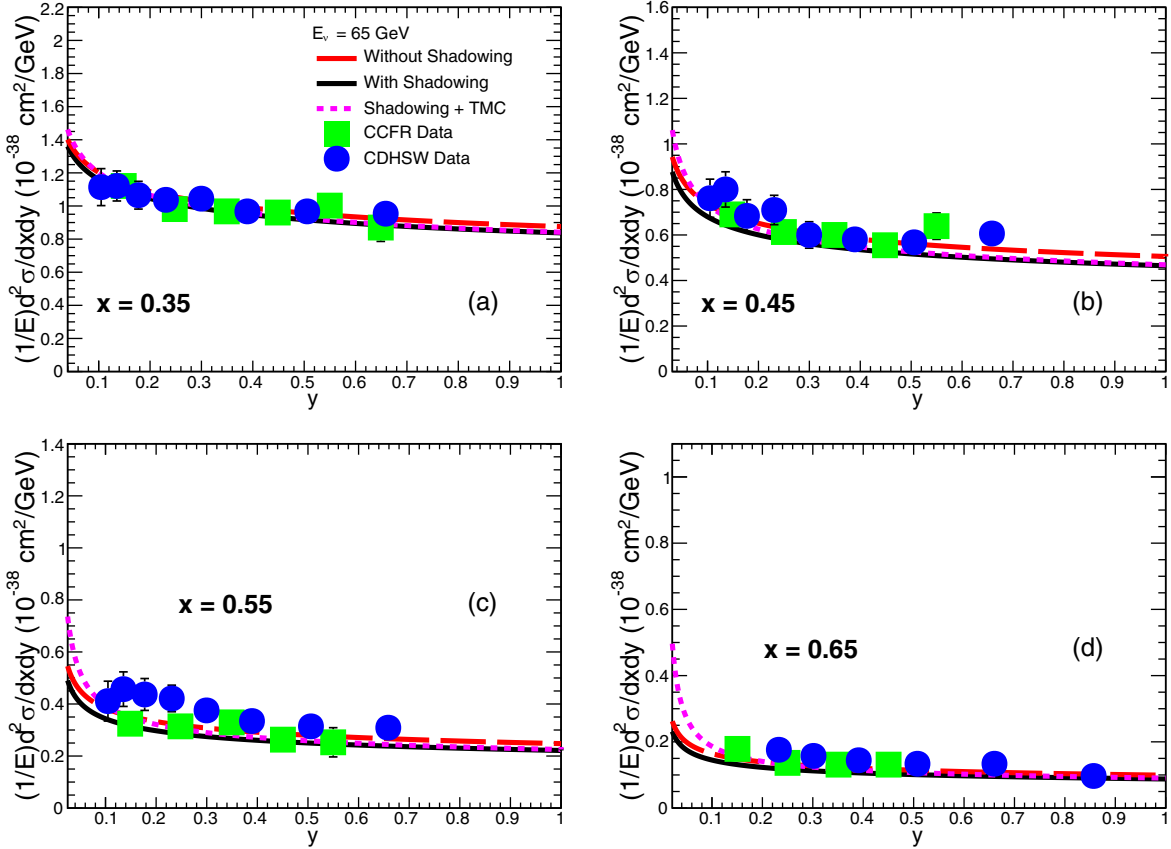


FIG. 8.  $\frac{1}{E} \frac{d^2\sigma}{dxdy}$  for  $^{56}\text{Fe}$  as a function of inelasticity  $y$ , for different values of the Bjorken variable  $x$  and  $E_{v\mu} = 65$  GeV using EPPS16 nuclear corrections [37] at NLO and LHAPDF (CT10) parton distribution functions [30]. Results are compared with measured data of the CCFR [41] and CDHSW [41] experiments.

The neutrino-nucleus (antineutrino-nucleus) charged current differential scattering cross section is defined as [36]

$$\begin{aligned} \frac{d^2\sigma_{CC}^{\nu(\bar{\nu})A}}{dx_A dy_A} &= \frac{G_F^2 M_A E_\nu}{\pi} \left( \frac{M_W^2}{Q^2 + M_W^2} \right)^2 \left[ y_A^2 x_A F_1^{\nu(\bar{\nu})A} \right. \\ &\quad + \left( 1 - y_A - \frac{M_A x_A y_A}{2E_\nu} \right) F_2^{\nu(\bar{\nu})A} \\ &\quad \left. \pm x_A y_A \left( 1 - \frac{y_A}{2} \right) F_3^{\nu(\bar{\nu})A} \right], \end{aligned} \quad (10)$$

where  $M_A$  is the mass of nucleus  $A$ .  $F_1^A$ ,  $F_2^A$ , and  $F_3^A$  are the structure functions for the nucleus. The Bjorken variable in the nucleus is  $x_A = x/A$ , where  $A$  is the mass number of the nucleus. The inelasticity in the nucleus is  $y_A = y$  [36].

To correct for the nuclear effects in the structure functions  $F_2^A$  and  $F_3^A$ , we use the EPPS16 package [37]. EPPS16 is a package to obtain next-to-leading order (NLO) nuclear partonic distribution functions (nPDFs). The bound nucleon PDFs  $f_i^A(x, Q^2)$  for each parton flavor  $i$  are given as

$$f_i^A(x, Q^2) = R_i^A(x, Q^2) f_i^{CT10}(x, Q^2), \quad (11)$$

where  $R_i^A(x, Q^2)$  are the nuclear corrections to the free nucleon PDFs  $f_i^{CT10}(x, Q^2)$ . EPPS16 provides parametrization

only in the kinematical domain  $1e - 7 \leq x \leq 1$  and  $1.3 \leq Q \leq 10000$  GeV.

The neutrino structure function  $F_3^A(x, Q^2)$  on nucleus  $A$  using EPPS16 [37] is calculated as

$$\begin{aligned} F_3^A(x, Q^2) &= u^A(x, Q) - \bar{u}^A(x, Q) + d^A(x, Q) \\ &\quad - \bar{d}^A(x, Q) + s^A(x, Q) - \bar{s}^A(x, Q) \\ &\quad + c^A(x, Q) - \bar{c}^A(x, Q) + b^A(x, Q) \\ &\quad - \bar{b}^A(x, Q) + t^A(x, Q) - \bar{t}^A(x, Q). \end{aligned} \quad (12)$$

The neutrino structure function  $F_2^A(x, Q^2)$  on nucleus  $A$  using EPPS16 [37] is calculated as

$$\begin{aligned} F_2^A(x, Q^2) &= x(u^A(x, Q) + \bar{u}^A(x, Q) + d^A(x, Q) \\ &\quad + \bar{d}^A(x, Q) + s^A(x, Q) + \bar{s}^A(x, Q) \\ &\quad + c^A(x, Q) + \bar{c}^A(x, Q) + b^A(x, Q) \\ &\quad + \bar{b}^A(x, Q) + t^A(x, Q) + \bar{t}^A(x, Q)). \end{aligned} \quad (13)$$

### Target-mass correction

The target-mass correction (TMC) can be taken into account when partonic distribution functions evaluate at the Nachtmann variable  $\xi$  [38] rather than the Bjorken variable

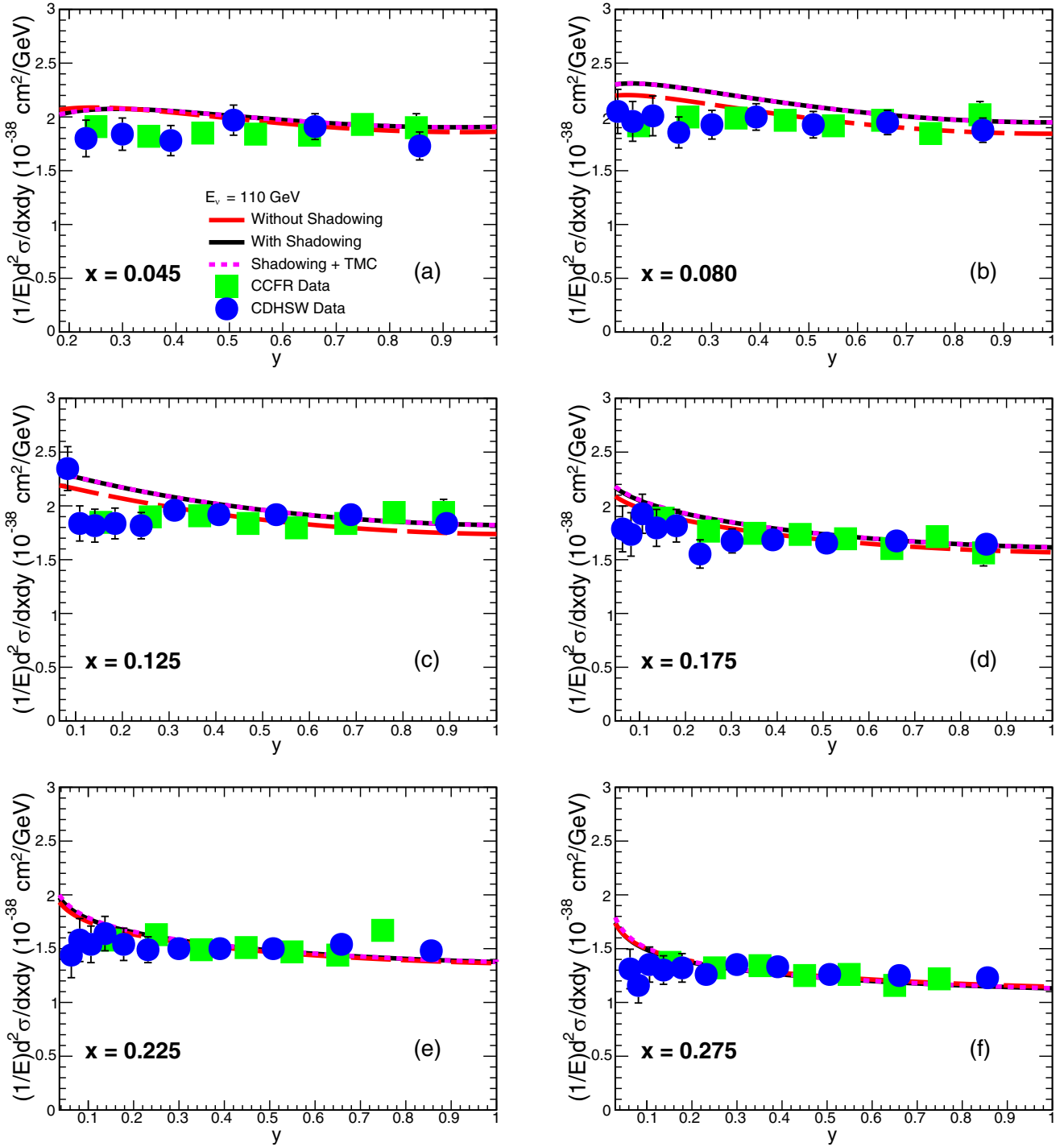


FIG. 9.  $\frac{1}{E} \frac{d^2\sigma}{dxdy}$  for  $^{56}\text{Fe}$  as a function of inelasticity  $y$ , for different values of the Bjorken variable  $x$  and  $E_{v_\mu} = 110$  GeV using EPPS16 nuclear corrections [37] at NLO and LHAPDF (CT10) parton distribution functions [30]. Results are compared with measured data of the CCFR [41] and CDHSW [41] experiments.

$x$  as

$$\xi = \frac{2x}{1 + \sqrt{1 + \frac{4M_N^2x^2}{Q^2}}}. \quad (14)$$

At high  $Q^2$  ( $Q^2 \gg M_N^2$ ),  $\xi$  is equivalent to  $x$ .

#### IV. RESULTS AND DISCUSSIONS

We calculated the structure functions  $F_2(x, Q^2)$  and  $x F_3(x, Q^2)$  for  $^{56}\text{Fe}$  with EPPS16 nuclear corrections [37] at next-to-leading order (NLO) and LHAPDF (CT10) parton distribution functions [30]. Figures 2 and 3 show present calculations of  $F_2(x, Q^2)$  as a function of the square of

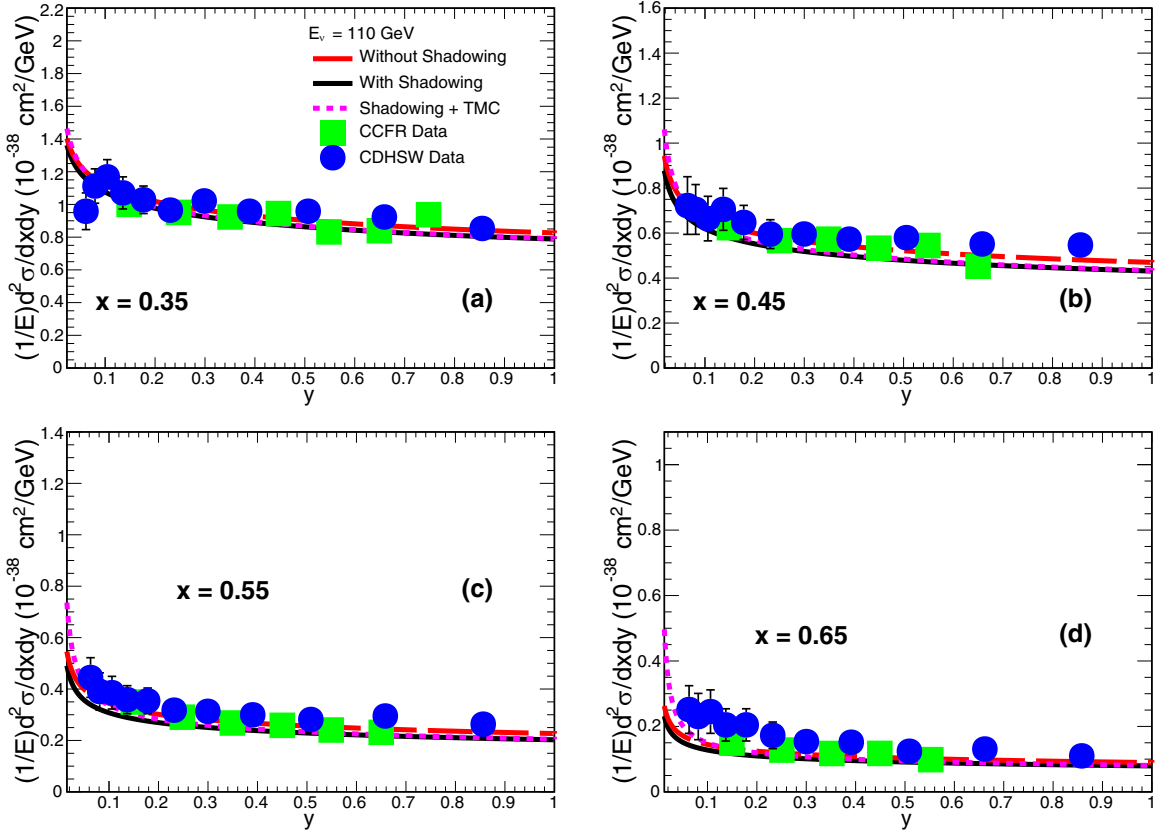


FIG. 10.  $\frac{1}{E} \frac{d^2\sigma}{dxdy}$  for  $^{56}\text{Fe}$  as a function of inelasticity  $y$ , for different values of Bjorken variable  $x$  and  $E_{v\mu} = 110$  GeV using EPPS16 nuclear corrections [37] at NLO and LHAPDF (CT10) parton distribution functions [30]. Results are compared with measured data of the CCFR [41] and CDHSW [41] experiments.

momentum transfer  $Q^2$  for different values of the Bjorken variable  $x$  (0.045, 0.080, 0.125, 0.175, 0.225, 0.275, 0.35, 0.45, 0.55, 0.65). Figures 4 and 5 show the present calculations of the structure function  $F_3(x, Q^2)$  as a function of the square of momentum transfer  $Q^2$  for different values of the Bjorken variable  $x$ . In Figs. 2 and 4, panel (a) is for  $x = 0.045$ , panel (b) is for  $x = 0.080$ , panel (c) is for  $x = 0.125$ , panel (d) is for  $x = 0.175$ , panel (e) is for  $x = 0.225$ , and panel (f) is for  $x = 0.275$ . In Figs. 3 and 5, panel (a) is for  $x = 0.35$ , panel (b) is for  $x = 0.45$ , panel (c) is for  $x = 0.55$ , and panel (d) is for  $x = 0.65$ . The black solid lines show the calculations with the inclusion of shadowing effect whereas the red dashed lines show the calculations without the inclusion of shadowing effect. The obtained results are compared with measured data of the CDHSW [39] and CCFR [40] experiments. We can see that, for higher values of the Bjorken variable  $x$ , the present theoretical approach gives a good description of the data. Figures 3(a) and 5(a) show an excellent agreement between theoretical calculations and data for  $x = 0.35$ .

Figure 6(a) shows the present calculations of the ratio  $R_2(x, Q^2) = F_2^{^{56}\text{Fe}}/F_2^{\text{Nucleon}}$  as a function of Bjorken variable  $x$  for  $Q^2 = 5.0$  GeV $^2$  and  $Q^2 = 50.0$  GeV $^2$ . Figure 6(b) shows present calculations of ratio  $R_3(x, Q^2) = F_3^{^{56}\text{Fe}}/F_3^{\text{Nucleon}}$  as a function of Bjorken variable  $x$  for  $Q^2 = 5.0$  GeV $^2$  and  $Q^2 = 50.0$  GeV $^2$ . The broken lines show the

effect of target mass correction [38]. We can clearly see the effects discussed in Sec. III.

We calculated  $\frac{1}{E} \frac{d^2\sigma}{dxdy}$  for  $^{56}\text{Fe}$  as a function of inelasticity  $y$ , for different values of Bjorken variable  $x$  and for different neutrino energies. Figures 7 and 8 show the present calculations of  $\frac{1}{E} \frac{d^2\sigma}{dxdy}$  for  $E_{v\mu} = 65$  GeV. Figures 9 and 10 show the calculations of  $\frac{1}{E} \frac{d^2\sigma}{dxdy}$  for  $E_{v\mu} = 110$  GeV. Figures 11 and 12 show the similar calculations of  $\frac{1}{E} \frac{d^2\sigma}{dxdy}$  for  $E_{v\mu} = 190$  GeV. The results obtained are compared with measured data of CCFR [41] and CDHSW [41] experiments. In Figs. 7, 9, and 11, panel (a) is for  $x = 0.045$ , panel (b) is for  $x = 0.080$ , panel (c) is for  $x = 0.125$ , panel (d) is for  $x = 0.175$ , panel (e) is for  $x = 0.225$ , and panel (f) is for  $x = 0.275$ . In Figs. 8, 10, and 12, panel (a) is for  $x = 0.35$ , panel (b) is for  $x = 0.45$ , panel (c) is for  $x = 0.55$ , and panel (d) is for  $x = 0.65$ . The black solid lines show the calculations with the inclusion of shadowing effect, the red dashed lines show the calculations without the inclusion of shadowing effect, and the pink dotted lines show the calculations with the inclusion of shadowing effect and target-mass correction. We can see that the target-mass correction has negligible effect at low values of the Bjorken variable  $x$ , but the effect increases with the increasing values of  $x$ . Also, TMC effects are seen for low values of inelasticity  $y$ . Here also we can see that, with the increasing

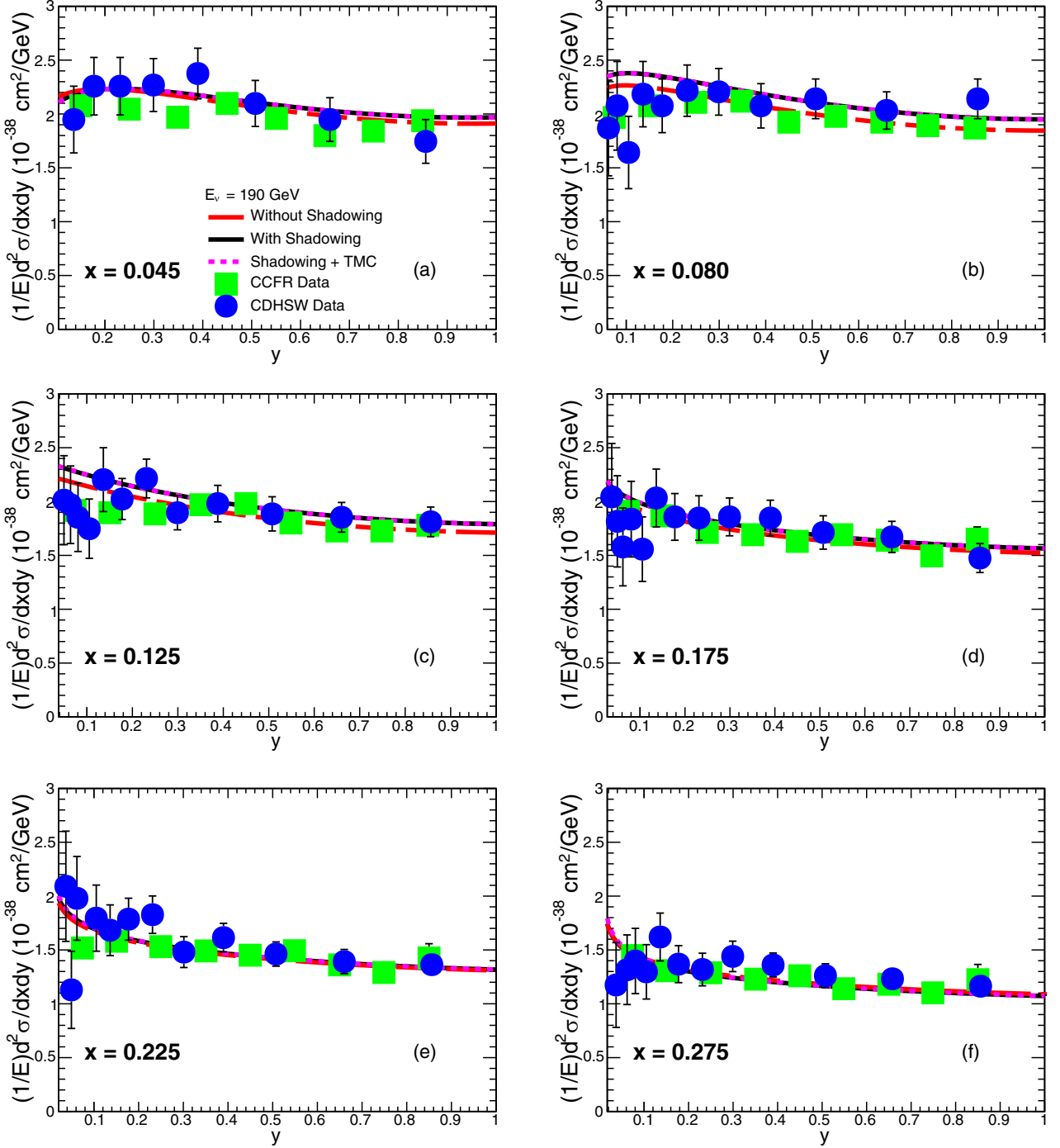


FIG. 11.  $\frac{1}{E} \frac{d^2\sigma}{dxdy}$  for  $^{56}\text{Fe}$  as a function of inelasticity  $y$ , for different values of Bjorken variable  $x$  and  $E_{v_\mu} = 190$  GeV using EPPS16 nuclear corrections [37] at NLO and LHAPDF (CT10) parton distribution functions [30]. Results are compared with measured data of the CCFR [41] and CDHSW [41] experiments.

values of  $x$ , theoretical calculations show a better agreement with data.

## V. CONCLUSION

We presented the structure functions [ $F_2(x, Q^2)$  and  $xF_3(x, Q^2)$ ], the ratios [ $R_2(x, Q^2) = F_2^{^{56}\text{Fe}} / F_2^{\text{Nucleon}}$  and

$R_3(x, Q^2) = F_3^{^{56}\text{Fe}} / F_3^{\text{Nucleon}}$ ] and the differential cross sections for charged current  $v_\mu$ —nucleon and  $v_\mu$ — $^{56}\text{Fe}$  deep-inelastic scattering by using a formalism based on the Hirai, Kumao, and Saito model. We used the LHAPDF (CT10) parton distribution functions. Nuclear corrections inside the nuclei are applied to the PDFs at next-to-leading order by using EPPS16 parametrization. We also incorporated

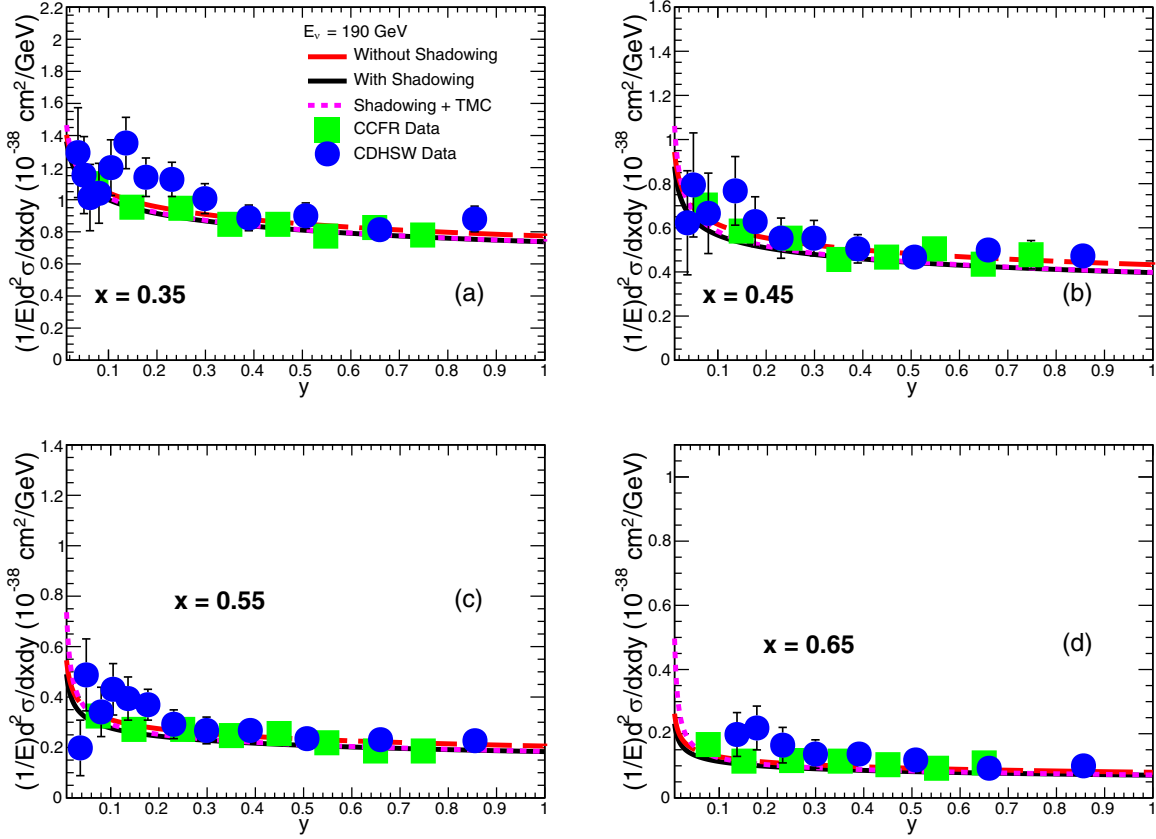


FIG. 12.  $\frac{1}{E} \frac{d^2\sigma}{dxdy}$  for  $^{56}\text{Fe}$  as a function of inelasticity  $y$ , for different values of Bjorken variable  $x$  and  $E_{v_\mu} = 190 \text{ GeV}$  using EPPS16 nuclear corrections [37] at NLO and LHAPDF (CT10) parton distribution functions [30]. Results are compared with measured data of the CCFR [41] and CDHSW [41] experiments.

target-mass correction into our calculations. We studied the behavior of the structure functions  $F_2(x, Q^2)$  and  $x F_3(x, Q^2)$  as a function of the square of momentum transfer  $Q^2$  for different values of the Bjorken variable  $x$ . Differential cross sections are analyzed as a function of inelasticity  $y$  for different values of the Bjorken variable  $x$  and for different neutrino energies. The results obtained have been compared with measured experimental data. The present theoretical approach gives a good description of data. The agreement

between theoretical calculations and data is even better for higher values of the Bjorken variable  $x$ .

## ACKNOWLEDGMENTS

The authors are thankful to Department of Science and Technology (DST), New Delhi, Government of India for the financial support needed to pursue this work.

- 
- [1] M. H. Ahn *et al.* (K2K Collaboration), *Phys. Rev. Lett.* **90**, 041801 (2003).
- [2] E. Aliu *et al.* (K2K Collaboration), *Phys. Rev. Lett.* **94**, 081802 (2005).
- [3] M. H. Ahn *et al.* (K2K Collaboration), *Phys. Rev. D* **74**, 072003 (2006).
- [4] Y. Ashie *et al.* (Super-Kamiokande Collaboration), *Phys. Rev. D* **71**, 112005 (2005).
- [5] Y. Takeuchi (Super-Kamiokande Collaboration), *Nucl. Phys. B Proc. Suppl.* **229-232**, 79 (2012).
- [6] P. Adamson *et al.* (NOvA Collaboration), *Phys. Rev. Lett.* **116**, 151806 (2016).
- [7] P. Adamson *et al.* (NOvA Collaboration), *Phys. Rev. D* **93**, 051104 (2016).
- [8] P. Adamson *et al.* (NOvA Collaboration), *Phys. Rev. Lett.* **118**, 151802 (2017).
- [9] P. Adamson *et al.* (NOvA Collaboration), *Phys. Rev. Lett.* **118**, 231801 (2017).
- [10] S. Ahmed *et al.* (ICAL Collaboration), *Pramana* **88**, 79 (2017).
- [11] D. Grover, K. Saraswat, P. Shukla, and V. Singh, *Chinese Phys. C* **42**, 123104 (2018).
- [12] K. Saraswat, P. Shukla, V. Kumar, and V. Singh, *Phys. Rev. C* **93**, 035504 (2016).

- [13] J. A. Formaggio and G. P. Zeller, *Rev. Mod. Phys.* **84**, 1307 (2012).
- [14] L. Alvarez-Ruso *et al.*, *Prog. Part. Nucl. Phys.* **100**, 1 (2018).
- [15] P. Lipari, *Nucl. Phys. B Proc. Suppl.* **112**, 274 (2002).
- [16] M. Tzanov, D. Naples, S. Boyd, J. McDonald, V. Radescu, R. A. Johnson, N. Suwonjandee, M. Vakili, J. Conrad, B. T. Fleming, J. Formaggio, J. H. Kim, S. Koutsoliotas, C. McNulty, A. Romosan, M. H. Shaevitz, P. Spentzouris, E. G. Stern, A. Vaitaitis, E. D. Zimmerman, R. H. Bernstein, L. Bugel, M. J. Lamm, W. Marsh, P. Nienaber, N. Tobien, J. Yu, T. Adams, A. Alton, T. Bolton, J. Goldman, M. Goncharov, L. deBarbaro, D. Buchholz, H. Schellman, G. P. Zeller, J. Brau, R. B. Drucker, R. Frey, D. Mason, S. Avvakumov, P. deBarbaro, A. Bodek, H. Budd, D. A. Harris, K. S. McFarland, W. K. Sakamoto, and U. K. Yang, *Phys. Rev. D* **74**, 012008 (2006).
- [17] G. Onengut *et al.* (CHORUS Collaboration), *Phys. Lett. B* **632**, 65 (2006).
- [18] Q. Wu *et al.* (NOMAD Collaboration), *Phys. Lett. B* **660**, 19 (2008).
- [19] D. Bhattacharya, Neutrino and antineutrino inclusive charged-current cross section measurement with the MINOS near detector, Ph.D. thesis, University of Pittsburgh, 2009; P. Adamson *et al.* (MINOS Collaboration), *Phys. Rev. D* **81**, 072002 (2010).
- [20] J. Mousseau *et al.* (MINERvA Collaboration), *Phys. Rev. D* **93**, 071101 (2016).
- [21] M. Tzanov, *AIP Conf. Proc.* **1222**, 243 (2010).
- [22] A. D. Martin, W. J. Stirling, R. S. Thorne, and G. Watt, *Eur. Phys. J. C* **63**, 189 (2009).
- [23] A. D. Martin, W. J. Stirling, R. S. Thorne, and G. Watt, *Eur. Phys. J. C* **64**, 653 (2009).
- [24] A. D. Martin, W. J. Stirling, R. S. Thorne, and G. Watt, *Eur. Phys. J. C* **70**, 51 (2010).
- [25] P. M. Nadolsky, H. L. Lai, Q. H. Cao, J. Huston, J. Pumplin, D. Stump, W. K. Tung, and C.-P. Yuan, *Phys. Rev. D* **78**, 013004 (2008).
- [26] S. Alekhin, J. Blümlein, and S. Moch, *Phys. Rev. D* **89**, 054028 (2014).
- [27] S. Alekhin, J. Blümlein, S. Moch, and R. Placakyte, *Phys. Rev. D* **94**, 114038 (2016).
- [28] S. Chekanov *et al.* (ZEUS Collaboration), *Phys. Rev. D* **67**, 012007 (2003).
- [29] M. R. Whalley, D. Bourilkov, and R. C. Group, [arXiv:hep-ph/0508110](https://arxiv.org/abs/hep-ph/0508110).
- [30] H. L. Lai, M. Guzzi, J. Huston, Z. Li, P. M. Nadolsky, J. Pumplin, and C.-P. Yuan, *Phys. Rev. D* **82**, 074024 (2010).
- [31] M. Hirai, S. Kumano, and K. Saito, *AIP Conf. Proc.* **1189**, 269 (2009).
- [32] C. G. Callan, Jr. and D. J. Gross, *Phys. Rev. Lett.* **22**, 156 (1969).
- [33] N. Armesto, *J. Phys. G* **32**, R367 (2006).
- [34] J. J. Aubert *et al.* (European Muon Collaboration), *Phys. Lett. B* **123**, 275 (1983).
- [35] M. Arneodo, *Phys. Rep.* **240**, 301 (1994).
- [36] H. Haider, I. R. Simo, and M. S. Athar, *Phys. Rev. C* **85**, 055201 (2012).
- [37] K. J. Eskola, P. Paakkinen, H. Paukkunen, and C. A. Salgado, *Eur. Phys. J. C* **77**, 163 (2017).
- [38] D. ChunGui, L. GuangLie, and S. PengNian, *Eur. Phys. J. C* **48**, 125 (2006).
- [39] J. P. Berge *et al.*, *Z. Phys. C: Part. Fields* **49**, 187 (1991).
- [40] E. Oltman *et al.*, *Z. Phys. C: Part. Fields* **53**, 51 (1992).
- [41] U. K. Yang, A Measurement of Differential Cross Sections in Charged Current Neutrino Interactions on Iron and a Global Structure Functions Analysis, Ph.D. thesis, Fermilab, 2001.